Crystalline lens radii of curvature from Purkinje and Scheimpflug imaging

4

4. Crystalline Lens radii of curvature from Purkinje and Scheimpflug imaging

This chapter is based on the article by P. Rosales et al., *"Crystalline Lens radii of curvature from Purkinje and Scheimpflug imaging"* Journal of Vision Vol 6(10), 1057-1067. Coauthors of the study are M. Dubbelman, S. Marcos and GL. Van der Heijde. The contribution of Patricia Rosales to the study was to adapt the Purkinje imaging system to do the comparison with Scheimpflug imaging, measurements of phakometry, data analysis of the Purkinje images and the discussion of the results after comparison between Purkinje and Scheimpflug imaging analysis data. Part of the study was conducted at VU Medical Center, the Vrije University, Amsterdam, The Netherlands Rob van der Heijde's lab.

RESUMEN

Objetivos: Comparación de las medidas de los radios de curvatura de las caras anterior y posterior del cristalino en estado desacomodado y en función de la demanda acomodativa (de 0 a 7D), medidos mediante los sistema de imágenes de Purkinje y de Scheimpflug corregida de distorsiones geométrica y óptica.

Métodos: La medida de los radios de curvatura del cristalino se realizó empleando un sistema de imágenes de Purkinje y una cámara de Scheimpflug corregida de distorsiones óptica y geométrica. Las medidas con ambos sistemas se realizaron en un mismo grupo de sujetos (46 ojos para la medida del radio de curvatura de la cara anterior del cristalino y 34 para la medida del radio de curvatura de la cara posterior del cristalino, ojos derechos en todos los casos) en estado desacomodado. También se realizó la comparación en función de la acomodación en 11 ojos. Las imágenes se procesaron empleando algoritmos propios, para la corrección de las distorsiones geométrica y óptica de la cámara de Scheimpflug y empleando los métodos del Teorema del Espejo Equivalente y una Función de Mérito para obtener los radios de curvatura del cristalino a partir de las imágenes de Purkinje. Las imágenes de Purkinje se analizaron teniendo en cuenta parámetros biométricos promedio (del modelo de ojo de Le Grand) y datos biométricos individuales obtenidos mediante la cámara de Scheimpflug. Los resultados obtenidos mediante ambos métodos se analizaron mediante un test ANOVA para medidas repetidas.

Resultados: Se evaluó la correlación entre el radio de la cara anterior del cristalino obtenidos mediante Scheimpflug y Purkinje utilizando correlaciones lineales y se obtuvieron pendientes, muy similares con ambos métodos (Teorema del Espejo Equivalente y Función de Mérito, empleando tanto datos biométricos individualizados como los del modelo de ojo), con pendiente entre 0.752 y 0.827; y r entre a 0.58 y 0.60, con una correlación estadísticamente significativa en todos los casos ($p < 0.0001$). Individualmente se encontraron diferencias

estadísticamente significativas entre ambas técnicas en 4 de los 46 ojos medidos (con datos biométricos individualizados) y en 10 ojos (con datos biométricos del modelo de ojo genérico), empleando el teorema del Espejo Equivalente (EE) y en 7 y 11 ojos respectivamente empleando la Función de Mérito (MF). En las correlaciones entre Scheimpflug y Purkinje para el radio de la cara posterior del cristalino se obtuvieron pendientes entre 1 y 1.09 y r entre 0.48 y 0.43, p<0.0001. Se encontraron diferencias estadísticamente significativas en 17 y 19 ojos de los 34 medidos empleando biometría individualizada y datos del modelo de ojo respectivamente, para el método del Espejo Equivalente y en 10 y 19 ojos respectivamente empleando la Función de Mérito. En el caso de los cambios de los radios de curvatura con la acomodación, con un análisis de la varianza (ANOVA) no se encontraron diferencias estadísticamente significativas ($F = 3.7$, $df = 1$, $p = 0.083$). Se encontró que el radio anterior del cristalino desacomodado, obtenido mediante las diferentes técnicas, empleando tanto datos biométricos como datos genéricos del modelo de ojo varía entre 7.23 ± 0.04 mm y 13.45 ± 0.59 mm para la cara anterior del cristalino y entre 4.73 ± 0.43 mm y 9.49 ± 0.18 mm para la cara posterior del cristalino. Ambas superficies se hacen más curvas con la acomodación, a razón de 0.59 mm/D para el radio anterior y 0.27 mm/D para el radio posterior, en promedio empleando las diferentes técnicas y empleando tanto datos biométricos individuales como genéricos del modelo de ojo.

Conclusiones: Con ambas técnicas se obtienen medidas rápidas y fiables de la curvatura del cristalino. Los datos obtenidos con la cámara de Scheimpflug son ligeramente menos variables que los obtenidos con las imágenes de Purkinje. Con la cámara de Scheimpflug, además, se puede obtener información mucho mas completa sobre la biometría de la cámara anterior y la geometría del cristalino. Sin embargo, es necesaria la dilatación de la pupila para mejorar la visibilidad de la cara posterior del cristalino que en algunos casos es imposible de detectar, mientras que con las imágenes de Purkinje ha sido posible realizar medidas robustas de la cara posterior del cristalino en todos los casos del estudio.

ABSTRACT

Purpose: We present a comparison between two methods to measure the radius of curvature of the anterior and posterior lens surfaces, corrected Scheimpflug Imaging and Purkinje Imaging in the same group of subjects (46 for the anterior lens, and 34 for the posterior lens). Comparisons were also made as a function of accommodation (0 to 7 D) in a subset of 11 eyes.

Methods: Data were captured and processed using laboratory prototypes and custom processing algorithms (for optical and geometrical distortion correction in the Scheimpflug system, and using either Equivalent Mirror or Merit Function methods for Purkinje). Analysis of Purkinje images was performed according to biometric parameters obtained from a model eye (Le Grand) and from individual biometric data obtained from Scheimpflug camera. Results from both methods are compared with an ANOVA test for repeated measurements.

Results: For anterior lens radius of curvature, slopes and correlation coefficients of a linear regression between anterior radii from Scheimpflug and Purkinje are very similar in all cases (slope ranging from 0.752 to 0.827, and r from 0.58 to 0.60), and the correlation is statistically significant in all cases ($p < 0.0001$). We found statistically significant differences in the anterior radii of curvature between techniques in 4 out of the 46 eyes (using individual biometry) and 10 eyes (using model eye data), with the Equivalent Mirror (EM) procedure, and 7 and 11 eyes respectively using the Merit Functon (MF). For the posterior lens radius of curvature we found statistically significant differences in the posterior radii of curvature. Slopes and correlation coefficients of a linear regresion between the posterior radius of curvature obtained with Scheimpflug and Purkinje imaging are very similar in all cases (ranging from a slope of 1 to 1.09, and r from 0.48 to 0.43, $p < 0.0001$). Differences between techniques were found in 17 and 19 out of 34 using individual biometry and model data respectively, for

the EM method, and in 10 and 9 subjects respectively for the MF. For lens radii of curvature during accommodation comparison, an analysis of variance (ANOVA) demonstrated that the difference in the anterior and posterior radius of curvature obtained with the two methods was not significant (F=3.7,df=1,p=0.083).

For the unaccommodated state, the average anterior lens radius of curvature with the different methos, using biometric data as well as data from the model eye was in the range between 7.23 ± 0.04 mm to 13.45±0.59 mm for the anterior lens radius of curvature and between 4.73 ±0.43 mm to 9.49±0.18 mm for the posterior lens radius of curvature. Both surfaces became more steeply curved with accommodation at a rate of 0.59 mm/D for the anterior lens radius of curvature and 0.27 mm/D for the posterior lens radius of curvature, on average using the different techniques and using custom biometric data as well as data from the model eye

Conclusions: Both techniques provided rapid and reliable data in a clinical/laboratory setting. Scheimpflug imaging is slightly less variable than Purkinje imaging and provides more complete information on anterior chamber biometry and the crystalline lens geometry, however it requires pupil dilation in order to improve the visibility of the posterior lens surface while with Purkinje imaging accurate measurement of the posterior lens surface is possible without pupil dilation.

1. INTRODUCTION

We have implemented techniques for phakometry measurements based on Purkinke imaging (with two different algorithms, the Equivalent Mirror Theorem and the Merit Function), and worked with images of the crystalline lens from Scheimpflug imaging systems. Despite Scheimpflug and Purkinje Imaging having been used by several authors to perform in vivo phakometry, to our knowledge a direct comparison between radii of curvature obtained with these two techniques on the same eyes has been never done. Koretz et al (Koretz, Strenk, Strenk & Semmlow, 2004) performed a comparative study between Scheimpflug and high-resolution magnetic resonance imaging (MRI) of the anterior segment of the eye. In that study each technique was performed on a different group of subjects, and only a comparison could be made on the trends of the cross-sectional changes with age. Furthermore, there has been discussion on the statistical methods used and the conclusions drawn from the results (Dubbelman, van der Heijde & Weeber, 2005). Cross-validation of Purkinje and Scheimpflug imaging on the same set of subjects during the same experimental session is important in order to validate both methods and shed light on the validity of both techniques on phakometry measurements.

In this chapter we compare phakometry from Purkinje imaging (developed at the Instituto de Optica, Madrid, and modified in order to obtain a similar configuration for fixation as the one used with Scheimpflug camera) and from a Scheimpflug imaging system (implemented at VU Medical Center, Amsterdam) on the same set of subjects for relaxed accommodation, and as a function of accommodation in a subsample of eyes. For comparison, Merit Function and Equivalent Mirror Theorem algorithms were evaluated, using custom biometric data from Scheimpflug imaging and model eye data from a Le Grand model eye to evaluate the accuracy of both methods and the influence of biometrical data on the precision of the measurement.

2. METHODS

2.1 Purkinje imaging.

The Purkinje imaging system developed in this thesis was used to perform phakometry. The optical set-up and data analysis, as well as experimental and computational validations, have been described in detail in Chapter 2. The system is

compact and was easily transported to the VU University Medical Center, Amsterdam, The Netherlands, where the experiments were conducted. For comparative measurements with the Scheimpflug system, a slight change was incorporated with respect to the described implementation used in other experiments: a mirror was inserted in the fixation channel in order to offer the left eye an accommodation stimulus, while the right eye is being imaged.

Heights of the double Purkinje images were computed and processed to obtain radii of curvature in the vertical meridian. The anterior and posterior lens radius of curvature were obtained using both the EM, (Smith & Garner, 1996) and the MF, methods (Garner, 1997), with custom-developed routines written in Matlab (detailed explanation of those methods is in Chapter 2). As described in that chapter, our typical experimental protocol involved measurement of corneal radius of curvature with videokeratography and optical biomety form the IOL master to process the data. In the study presented in this chapter, we obtained both optical biometry and anterior cornea radius of curvature from Scheimpflug imaging or constant data from a model eye and both results are reported.

2.2 Scheimpflug imaging

The set-up of the Scheimpflug camera as well as the necessary corrections of the Scheimpflug images, implemented at the VU Medical Center in Amsterdam, has been described previously in detail (Dubbelman M, Sicam VA & van der Heijde G. L, 2006, Dubbelman M, van der Heijde G.L & HA., 2001, Dubbelman et al., 2005), and in Chapter 3. Images were obtained with the Topcon SL-45 Scheimpflug camera, the film of which was replaced by a CCD-camera. Correction and analysis of the Scheimpflug images were done using custom developed software as described in Chapter 3. Conic of revolution were fitted to the anterior and posterior lens surfaces in order to find the asphericities of the surfaces. Furthermore, a circle was fitted to the central 3 mm zone of both lens surfaces and it is this radius of curvature that will be compared with the results of the Purkinje imaging. As a result, at least 3 mm of the lens surface should be visible on the Scheimpflug image in order to obtain its radius of curvature. For the posterior lens surface, this was not always the case, especially when only phenylephrine was used to dilate the pupil. Dubbelmann (Dubbelman & van der Heijde, 2001) validated the method in vitro, with an artificial eye and in vivo with four subjects with intraocular

lenses. The combination of the reproducibility and systematic errors has been estimated as approximately 0.3 mm for the anterior lens and 0.25 mm for the posterior lens surface.

2.3 Subjects

Experiments were performed on the right eye of 46 normal subjects with ages ranging between 22 and 60 years (30 ± 9 yrs, mean and standard deviation). Spherical equivalent ranged from -7.25 to 4.25 D (-1.5 ± 2.5 D). The experimental protocols followed the tenets of the declaration of Helsinki and had been approved by institutional review boards. Subjects were informed on the nature of the experiments and provided written consent.

A sub-sample of 11 subjects (ages ranging from 22 to 36 years, mean 28.5 years) was also examined as a function of accommodation stimulus.

2.4 Experimental procedures

The right eye of the subjects was dilated with one drop of tropicamide and one drop of 5% phenylephrine HCl. For those 11 subjects who were also measured as a function of accommodation stimulus, only two drops of 5% phenylephrine were used. Subsequently, refractive error and keratometry was measured with a Topcon KR-3500 autokerato-refractometer. Purkinje and Scheimpflug measurements were obtained in turns in the same experimental session. The subject was seated with the head in upright position, and the slit beam of the Scheimpflug was vertically oriented. The left eye was used to focus a fixation stimulus, while the right eye was photographed. The fixation stimulus was an illuminated black Maltese star (diameter: 5 cm), which was located 0.5 m from the left eye. Refractive error was corrected with trial lenses in a lens holder directly in front of the left eye and a +2 D lens was added as well in order to obtain the unaccommodated state of the eye. Subjects wearing contact lenses kept the left lens in. First of all, the subject fixated with the right eye the fixation light in the Scheimpflug camera, while the slit of the camera was aligned along the optical axis of the right eye. Then, the subject fixated with the left eye the Maltese star, the position of which can be adjusted horizontally and vertically by a remote control until the subject reports that the fixation light of the Scheimpflug camera is superimposed on the center of the Maltese star. Subsequently, the internal fixation light of the camera was turned off. At that time,

the subject was asked to focus on the Maltese star and two images were obtained. For 11 subjects, Scheimpflug images of the right eye were also obtained as a function of accommodation. For these images, the same procedure was followed except for the fact that in order to induce accommodation the power of the lens in front of the left eye was reduced in steps of 1 D with the trial lenses. Measurements were performed until the subject indicated that it was no longer possible to focus sharply on the star.

Purkinje images were obtained with the double vertical LEDs. The right eye's pupil was aligned to the optical axis of the camera by means of a X-Y-Z stage to which a chin rest was mounted. For the left eye, the set-up (lens holder, trial lenses, Maltese cross) and protocol for the accommodation experiments were identical to that used during the Scheimpflug imaging. The pupil was continuously monitored to ensure centration and convergence was corrected by changing the lateral position of the Maltese star, until the pupil was in the center of the screen.

Each measurement was repeated at least three times for each method for statistical analysis.

2.5 Statistical analysis

Statistical differences of the radii of curvature between techniques for the global sample were tested using a general linear model and analysis of variance (ANOVA) for repeated measurements. To test statistical differences between techniques for each individual eye we performed a Test of Homogeneity of Variances (for repeated measurements with the same technique). As a result, we applied ANOVA with the Bonferroni post hoc test if the variances were equal and Welch-ANOVA with the Tamhane post hoc test if the variances were unequal. The change of radii of curvature with accommodation, and differences of those between techniques were tested using ANOVA. In all cases a significance level (p) of 0.05 was considered (or a confidence interval of 95%).

3. RESULTS

Figure 4.1 shows a typical example of a Purkinje image showing double PI, PIII and PIV (A) and an example of a corrected Scheimpflug image (B), for the same unaccommodated eye.
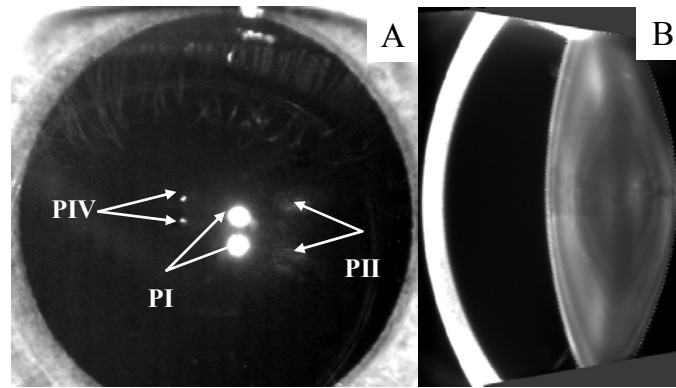
Figure 4.1. Examples of **A.** Purkinje Images **B.** Scheimpflug Image for the same unaccommodated eye.

3.1 Lens radii of curvature of the unaccommodated eye

Table 4.1 shows that there is a good match between anterior lens radius of curvature measurement from Purkinje imaging and Scheimpflug imaging.

Anterior Lens Radius	SCHEIMP FLUG CAMERA	PURKINJE IMAGING SYSTEM			
		Individual Biometric Data (I)		Model Eye (ME)	
		MF	EM	MF	EM
Average	11.1 ± 1.1	10.8 ± 1.1	10.95 ± 1.1	10.8 ± 1.3	10.9± 1.25
Range	[8.1, 13.8]	[7.9 , 13.3]	[8.1 , 13.6]	[7.2 , 13.45]	[7.4 , 13.5]

Table 4.1. Comparison of the anterior lens radii of curvature in mm (mean and standard deviation) obtained with Scheimpflug and Purkinje imaging.

There are no significant differences between Purkinje imaging anterior radii with data processed using individual biometric (I) or model eye data (LG) (p=0.072 for EM, and p=0.113 for MF). The average (±SD) difference between the anterior lens radius of curvature obtained with Scheimpflug and Purkinje imaging is 0.36 ±0.76mm (MF) and 0.13 ±0.77mm (EM).
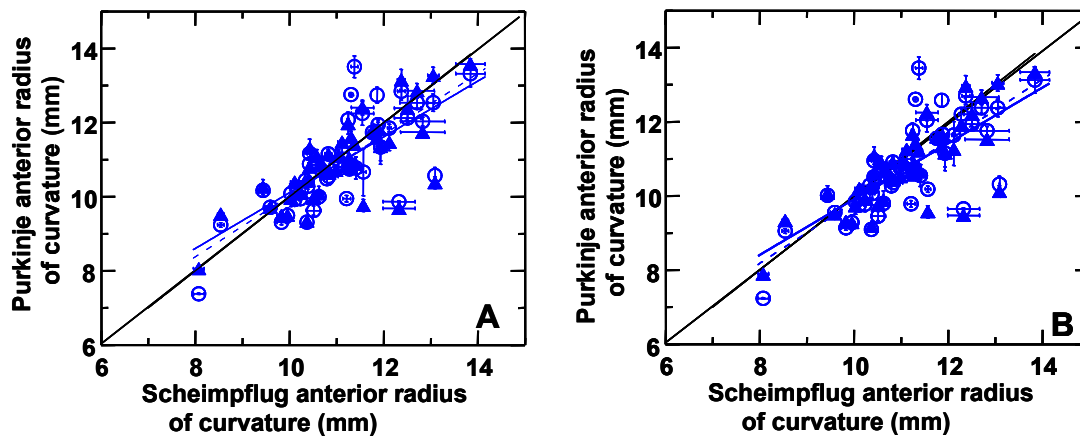
Figure 4.2. Anterior radii of curvature from Scheimpflug imaging vs Purkinje imaging using **A.** Equivalent Mirror **B.** Merit function. Solid triangles are for Purkinje imaging using individual biometry and open circles using biometry from a model eye. It is remarkable the similarity between both graphics.

Figure 4.2 A shows the anterior lens radii of curvature obtained from Scheimpflug measurements versus those obtained from Purkinje imaging using the EM theorem. Solid symbols are for Purkinje imaging data using individual biometric data of anterior chamber depth and lens thickness, and open symbols are for Purkinje imaging data using fixed data from the model eye. Similarly, Figure 4.2 B shows the same data, but with Purkinje imaging using the Merit Function (MF) algorithm. In this figure, vertical error bars represent individual variability (standard deviation) for repeated Purkinje imaging anterior radii estimates. Average (across-subjects) standard deviation for repeated measurements was 0.5 mm. This variability arises from an average measurement variability in h_3 (separation of PIII double images) and h_1 (separation of PI double images) of 0.11 mm in both cases. Horizontal error bars represent individual variability for repeated Scheimpflug imaging (and was 0.10 mm on average).

Slopes and correlation coefficients of a linear regression between anterior radii from Scheimpflug and Purkinje are very similar in all cases (slope ranging from 0.752 to 0.827, and r from 0.58 to 0.60), and the correlation is statistically significant in all cases ($p< 0.0001$). In an ANOVA for repeated measurements the difference across the entire sample was not statistically significant using the EM (for both individual biometry, $p=0.221$ and model eye biometry, $p=0.231$). This statistical test found differences for the MF ($p=0.003$ and $p=0.011$ for individual and model eye biometry, respectively). On an individual basis, we found statistically significant differences in the anterior radii of

curvature between techniques in 4 out of the 46 eyes (using individual biometry) and 10 eyes (using model data), with the EM procedure, and 7 and 11 eyes respectively using the MF.

Table 4.2. Comparison of the posterior lens radii of curvature in mm (mean and standard deviation) obtained with Scheimpflug and Purkinje imaging**.**

Posterior Lens Radius	SCHEIMPFLUG CAMERA	PURKINJE IMAGING SYSTEM			
		Individual Biometric Data		Model Eye	
		MF	EM	MF	EM
Average	6.1 ± 0.55	6.7 ± 0.8	7.6 ± 1.0	6.5 ± 1.0	7.4 ± 1.2
Range	[5.1 , 7.15]	[5.2 , 8.65]	[5.7 , 10.2]	[4.8 , 9.5]	[5.2 , 11.15]

Table 4.2 shows posterior lens radii of curvature (average ± SD and range) obtained from Scheimpflug, and Purkinje imaging (with the MF, and EM, and individual phakometry, I, or model eye data, LG, respectively). Unlike results for the anterior lens, posterior lens radii of curvature from the MF and EM are significantly different. The average (±SD) differences between the posterior lens radius of curvature obtained with Scheimpflug and Purkinje imaging are -0.57 ± 0.58 mm (MF) and -1.47± 0.84 mm (EM). The difference is not increased when using non-individual data (-0.42 mm), as can be seen in Table 4.2.
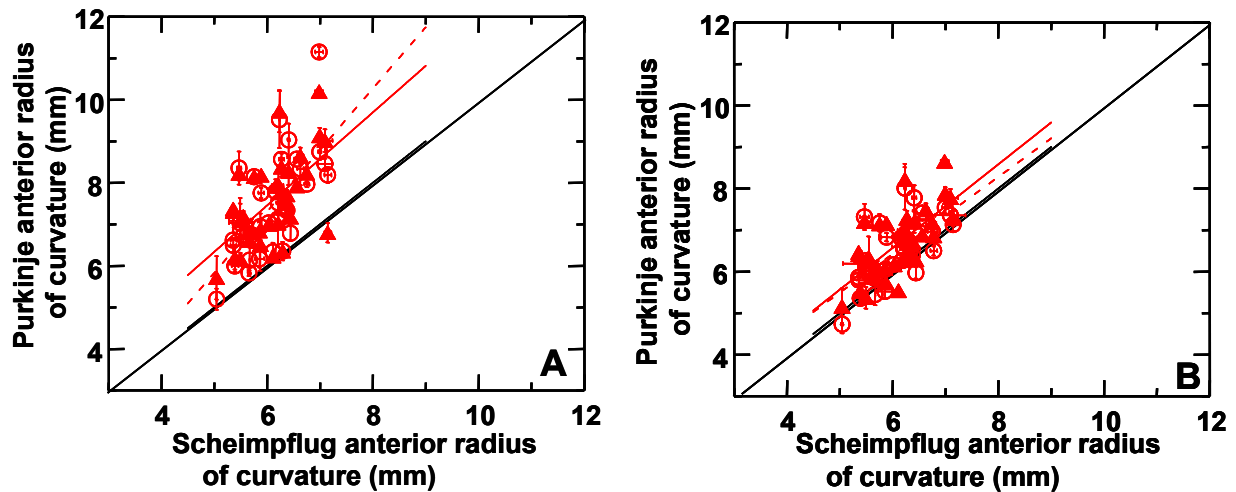
Figure 4.3. Posterior radii of curvature from Scheimpflug imaging vs Purkinje imaging using **A.** Equivalent Mirror **B.** Merit Function. Solid triangles are for Purkinje imaging using individual biometry and open circles are for Purkinje imaging using biometry from a model eye.

Figure 4.3 shows posterior radii of curvature from Scheimpflug imaging versus Purkinje imaging in a similar format to that of Figure 4.2. For simplicity, we show absolute values, whereas the posterior radii of curvature are always negative. Vertical error bars represent individual variability (standard deviation) for repeated Purkinje imaging posterior radii estimates. Average (across-subjects) standard deviation for repeated measurements was 0.31 mm. This variability arises from a average variability in h_4 (separation of PIV double images) and h_1 (separation of PI double images) measurements of 0.02 mm in both cases. Horizontal error bars represent individual variability for repeated Scheimpflug imaging (and was 0.22 mm on average).

We have also estimated the differences in crystalline lens surface power resulting from the differences in anterior and posterior radii of curvature across techniques. We have used the lens maker formula, using individual data of lens thickness and equivalent refractive index obtained from Scheimpflug. For MF and LG we estimated that Purkinje/Scheimpflug differences in anterior lens radius of curvature of 0.3 mm and posterior lens radius of curvature of −0.45 mm will result in differences in lens power of 0.61 D.

Slopes and correlation coefficients of linear regressions between the posterior radius of curvature obtained with Scheimpflug and Purkinje imaging are very similar in all cases (ranging from a slope of 1 to 1.09, and r from 0.48 to 0.43, p<0.0001). In an analysis of variance the difference across the entire samples was statistically significant, for both the EM and MF (p<0.01 in all cases). On an individual basis, we found statistically significant differences in the posterior radii of curvature between techniques in 17 and 19 out of 34 using individual biometry and model data respectively, for the EM method, and in 10 and 9 subjects, respectively, for the MF.

3.2 Lens radius of curvature during accommodation

Figure 4.4 shows changes in the anterior and posterior radius of curvature as a function of accommodation in the same eyes for three subjects of whom it was possible to measure the radius of curvature of the posterior lens surface across the full accommodative range. All Purkinje imaging data are for the MF algorithm. No significant differences were found between using individual or model biometric data, despite the fact that ACD and lens thickness vary significantly with accommodation. Both the radius of curvature of the anterior and posterior lens surface show similar trends individually, although for some individual subjects there seems to be an almost

constant offset (for example anterior radius of curvature for S1, or posterior radius of curvature for S7).
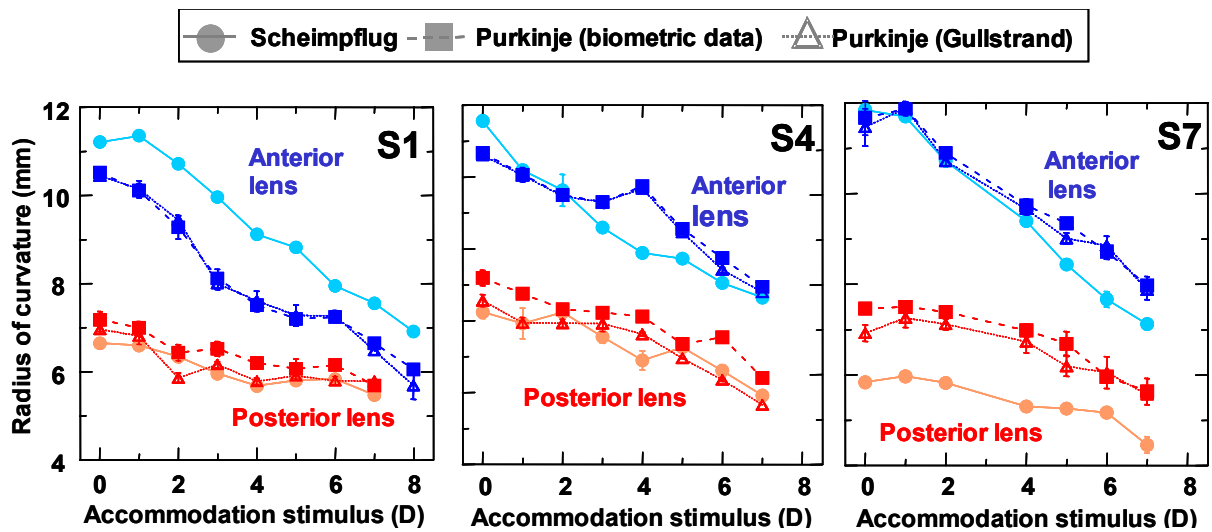
Figure 4.4. Change of anterior and posterior lens radii of curvature as a function of accommodation in three individual eyes. Each colour stands for a different subject.
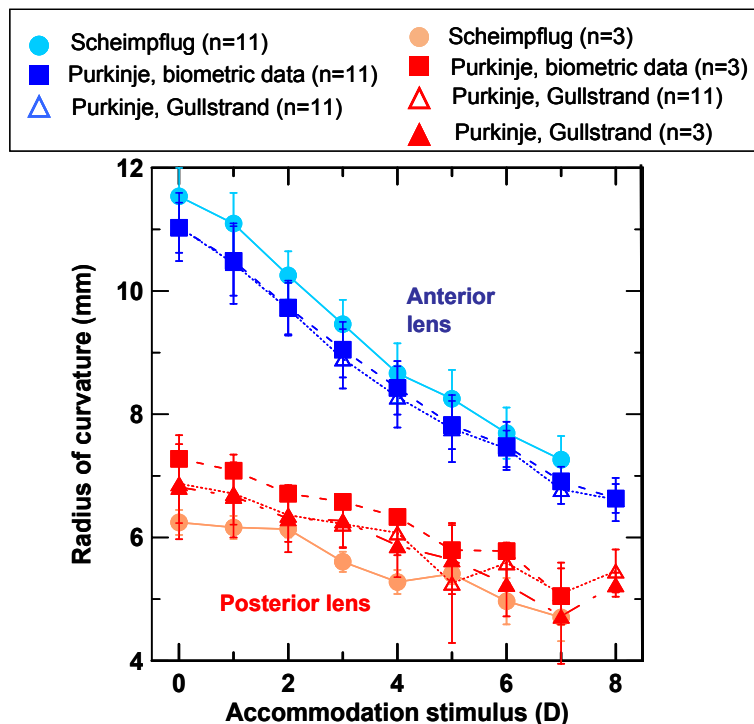
Figure 4.5. Change of anterior and posterior lens radius of curvature as a function of accommodation, averaged across eyes.

We did not observe a consistent trend of Scheimpflug/Purkinje discrepancy as a function of accommodation (Figure 4.5). For the anterior lens, the Purkinje radii were slightly lower than those of the Scheimpflug in all eyes (on average across subjects and accommodation by 0.39±012 mm and 0.46±014 mm, using individual biometry and

model eye data respectively). For the posterior lens, the Purkinje radii were slightly higher than those of the Scheimpflug in all eyes (average ± SD. across subjects and accommodation was 0.38±0.24mm). Table 4.3 shows the range of variation of anterior and posterior radii of curvature from 0 to 8 D of accommodation and slope of the linear regresion to the data using Scheimpflug and Purkinje imaging.

In an analysis of variance (ANOVA) the difference in the anterior and posterior curvature radius of curvature obtained with the two methods was not significant ($F = 3.7$, df = 1, $p = 0.083$) whereas the difference of radii of curvature across the different accommodative states was significant ($F = 231.8$, df = 6, $p < 0.001$).

Table 4.3. Range of variation of the anterior and posterior radii of curvature between 0 and 8 D and slope of the linear regression to the data, from Scheimpflug and Purkinje imaging.

	SCHEIMPFLUG	PURKINJE IMAGING SYSTEM (MF)	
		Individual Biometry	Model Eye
ANTERIOR LENS RADIUS (mm)			
Range	(11.54, 7.26)	(11.03, 6.9)	(11.04, 6.78)
slope	-0.64	-0.57	-0.57
POSTERIOR LENS RADIUS (mm)			
Range	(6.24, 4.7)	(7.28, 5.05)	(6.81, 5.23)
slope	-0.23	-0.29	-0.29

4. DISCUSSION

We found good correspondence of lens radii of curvature with our implementations of Scheimpflug and Purkinje imaging systems on the same group of eyes. The ranges of radii of curvature found with both techniques are consistent to those reported before in normal eyes for the unaccommodated eye and under different levels of accommodation stimuli. Although previous studies on different populations and different experimental protocols, and the lack of a gold standard for calibration, prevented validation of the accuracy of the different techniques used for phakometry, our comparison on an individual basis allows us to identify potential systematic errors associated to a given technique and assess the potential advantages or limitations of the different techniques.

We found that Scheimpflug and Purkinje imaging (with EM) provided statistically similar results for the anterior radius of curvature. We have also shown that using individual biometry data increases slightly the similarity between techniques for the anterior radius of curvature, and only marginally for the posterior radius of curvature, with respect of using general data from the model eye.

We have performed computer simulations to assess whether there are systematic differences that can be attributed to the Purkinje imaging method, or whether the errors do not follow any particular trend and can be attributed to both methods. The details of the ray tracing of our apparatus and computer simulations of Purkinje images were described in the Chapter 2 of this thesis. In brief, we simulated with Zemax the configuration of the optical system and simulated the intensity distributions of the Purkinje images for a model eye. The simulated Purkinje images were processed as the experimental images, using the MF. For the present simulations, we used as nominal values for the model eyes (biometry and radii of curvature of the cornea and anterior and posterior lens) those obtained from Scheimpflug imaging. We performed simulations for model eyes with spherical surfaces (as assumed in the processing algorithms) and also aspherical surfaces, with asphericities (Q-values) obtained from Scheimpflug imaging in each individual eye (-0.26 ± 0.19 for the anterior cornea, -0.49 ± 0.19 for the posterior cornea, -2.00 ± 0.15 for the anterior lens, -2.65 ± 1.42 for the posterior lens). The simulations were performed for 31 eyes. For the anterior radii of curvature, predictions using spherical surfaces in the model eye reveal a slight underestimation of Purkinje radii compared to Scheimpflug radii of curvature (nominal values in the model). However, similarly to the experimental findings, these differences are not significant. The average differences between Purkinje imaging and Scheimpflug anterior radii of curvature were 0.28±0.67 mm for the experimental values in these set of eyes, -0.50±0.16 mm for the predicted values using spherical surfaces and –0.34±0.25 mm for the predicted values using aspherical surfaces. There are good correlations between Scheimplug and Purkinje data. For the spherical surface model, we found a slope closer to 1 (0.93) than for the experimental (0.81) or predictions (0.87) using the aspheric model. For the posterior radius of curvature predictions with the aspheric model reproduce a systematic overestimation of Purkinje imaging data from the nominal Scheimpflug data. A lower overestimation is found for the spherical model eye. The average differences between Purkinje imaging and Scheimpflug posterior radii of curvature were 0.60±0.57 mm for the experimental values, 0.48±0.43 mm for the predicted values using spherical surfaces, and 1.04±0.69 mm for the predicted values using aspherical surfaces. These simulations indicate that the discrepancies found between the Purkinje and Scheimpflug posterior radii are partly inherent to the method, and also to the fact that the surface of the crystalline lens is not spherical, but exhibits a

negative asphericity (with nominal values obtained from Scheimpflug). The larger the asphericity, the larger the discrepancy. Thus, the simulations predict a higher overestimation of the lens radii respect to nominal values, whereas the experimental values lie in between predictions from spherical and aspheric surfaces. This could indicate that the asphericity of the lens is actually lower (more spherical) or that the gradient index of the lens could play a counteractive role. The asphericity of the anterior surface does not seem to affect the estimation of the anterior lens radius of curvature using Purkinje imaging, but the asphericity of the anterior lens surface, posterior lens surface, or both, do play a substantial large role in the slight overestimation of the Purkinje radii of curvature. The asphericity of the crystalline lens surfaces in young eyes is usually negative (Dubbelman et al., 2005), but varies significantly across subjects, and as a function of accommodation. The MF could incorporate an aspheric eye model to account for some of this effect, although a fixed asphericity will probably not account for all the individual effects.